NASA TECHNICAL NOTE

NASA TN D-5086

c. 1

NASA TN D-5086

EXPERIMENTAL DETERMINATION OF EDDY-CURRENT TORQUES ON BODIES ROTATING RELATIVE TO A UNIFORM MAGNETIC FIELD

by J. C. Boyle, E. J. Mosher, and J. M. Greyerbiehl

Goddard Space Flight Center
Greenbelt, Md.

NATIONAL AERONAUTICS AND SPACE ADMINISTRATION • WASHINGTON, D. C. • JULY 1969

NASA TN D-5086

EXPERIMENTAL DETERMINATION OF EDDY-CURRENT TORQUES ON BODIES ROTATING RELATIVE TO A UNIFORM MAGNETIC FIELD

By J. C. Boyle, E. J. Mosher,
and J. M. Greyerbiehl

Goddard Space Flight Center
Greenbelt, Md.

NATIONAL AERONAUTICS AND SPACE ADMINISTRATION

For sale by the Clearinghouse for Federal Scientific and Technical Information
Springfield, Virginia 22151 – CFSTI price $3.00

ABSTRACT

This report presents eddy-current torque measurements made on conducting bodies of various shapes. The results obtained are compared with available theory as well as with the findings of other experimenters. A novel feature of this program is that the test specimens were held stationary while the magnetic field was rotated. This not only eliminated problems of windage and bearing friction, but permitted extension of the tests into higher frequency ranges than had previously been investigated. Also included is a brief discussion of the implications to present and future spacecraft.

CONTENTS

EXPERIMENTAL DETERMINATION OF EDDY-CURRENT TORQUES ON BODIES ROTATING RELATIVE TO A UNIFORM MAGNETIC FIELD

by
J. C. Boyle, E. J. Mosher
and J. M. Greyerbiehl
Goddard Space Flight Center

A conducting body rotating within a magnetic field will have eddy currents induced in it. The resultant magnetic field from these eddy currents interacts with the initial field to produce torques tending to despin and precess the rotating body. This phenomenon is of interest in the case of satellites spinning in the earth's magnetic field or using attitude control reaction wheels; it is of potential interest to future missions such as a Jupiter probe or orbiter.

Theoretical analysis of eddy-current torques involves complex mathematics, and most treatments assume that the body is rotating slowly enough that distortion of the ambient field caused by the induced currents is negligible.

A number of experimenters (References 1 and 2) have performed spin-decay experiments to verify the low rotational frequency theory. The objective here has been to extend this work to higher frequencies and to different geometries, and to compare the results with existing theory.

In general, eddy currents will produce both despin and precessional torque components. In this investigation, only despin torques were considered.

PREVIOUS INVESTIGATIONS

Theoretical

A survey of published literature discloses that eddy-current torque formulas of unrestricted rotational frequency range exist for both sphere and thin-walled cylinder of infinite length (References 3 and 4). Field distortion effects are included in these studies.

A number of authors (References 5, 6, 7, and 8) have calculated torques on the assumption of no field distortion, i.e., for low frequencies. Formulas are available for spheres, for both open- and closed-end circular cylinders of finite length, and for cones, cone frustums, and general bodies of revolution. The torque formulas obtained by the various authors are presented in Table 1.

Table 1

Eddy-Current Torque Formulas for Thin Shell Bodies Revolving About an Axis Normal to a Magnetic Field, Rewritten with Common Terminology.

Configuration	Smythe (Reference 3)	Smith (Reference 6)	Bredart (Reference 8)	Hooper (Reference 5)	Wilson (Reference 7)
Sphere	$\frac{6\pi B^2 S \omega r^4}{9S^2 + \mu_v^2 r^2 \omega^2}$	None	$\frac{2\pi B^2 r^4 \omega}{3S}$	$\frac{160 B^2 r^4 \omega}{75S}$	$\frac{2\pi B^2 r^4 \omega}{3S}$
Vertical Open Cylinder	$\frac{4\pi \omega S r^3 B^2}{4S^2 + \omega^2 \mu_v^2 r^2}$ *	$\frac{\pi B^2 \omega r^3 \ell}{S\left(1 - \frac{2r}{\ell} \text{TANH} \frac{\ell}{2r}\right)^{-1}}$	$\frac{\pi B^2 \omega r^3 \ell}{S\left(1 - \frac{2r}{\ell} \text{TANH} \frac{\ell}{2r}\right)^{-1}}$	$\frac{\pi B^2 \omega \ell^2 r^3}{S\left(\ell + \frac{\pi r}{2}\right)}$	None
Vertical Closed Cylinder	$\frac{4\pi \omega S r^3 B^2}{4S^2 + \omega^2 \mu_v^2 r^2}$ *	None	$\frac{\pi \omega B^2 r^3 \ell}{S\left(1 - \frac{\frac{2r}{\ell} \text{TANH} \frac{\ell}{2r}}{1 + \text{TANH} \frac{\ell}{2r}}\right)^{-1}}$	$\frac{\pi B^2 \ell^2 r^3 \omega}{S(\ell + 2r)}$	$\frac{2r}{\ell} < 1$ $\frac{2B^2 \omega \ell^3 r}{S}\left[\frac{\pi}{4}\left(\frac{3\ell}{2r} + 1 + \frac{r}{\ell}\right) - \left(1 + \frac{1}{2 - \frac{4r}{\ell}}\right) - \frac{3 - \frac{8r}{\ell}}{\frac{2r}{\ell}\left(1 - \frac{2r}{\ell}\right)\sqrt{1 - \frac{4r^2}{\ell^2}}} \text{TAN}^{-1} \frac{\sqrt{1 - \frac{4r^2}{\ell^2}}}{1 + \frac{2r}{\ell}}\right]$ $\frac{2r}{\ell} > 1$ $\frac{2B^2 \omega \ell^3 r}{S}\left[\frac{\pi}{4}\left(\frac{3\ell}{2r} + 1 + \frac{r}{\ell}\right) - \left(1 + \frac{1}{2 - \frac{4r}{\ell}}\right) - \frac{3 - \frac{8r}{\ell}}{\frac{4r}{\ell}\left(1 - \frac{2r}{\ell}\right)\sqrt{\frac{4r^2}{\ell^2} - 1}} \text{LOG}_e\left(\frac{2r}{\ell} + \sqrt{\frac{4r^2}{\ell^2} - 1}\right)\right]$ $\frac{2r}{\ell} \quad 1$ $\left(18\pi - \frac{160}{3}\right)\frac{B^2 \omega r^4}{S}$
Horizontal Closed Cylinder	None	None	None	None	$\frac{1}{2}$ Corresponding Value of Vertical Cylinder Plus $\frac{\pi B^2 \omega}{4S}\left(\frac{r}{2} + \ell\right) r^3$
Horizontal Open Cylinder	None	$\frac{\pi B^2 \omega r^3 \ell}{2S\left(1 - \frac{2r}{\ell} \text{TANH} \frac{\ell}{2r}\right)^{-1}}$	None	None	None

*Torque per unit length for an infinite length.

Experimental

Eddy-current damping has been measured in the laboratory by Juergensen, Sanduleak, and Teuber (Reference 2); and by Eide (Reference 1). Both of these investigations were made with the test specimens spinning in a fixed magnetic field. Damping torques and coefficients were computed from spin decay. Juergensen, Sanduleak, and Teuber tested cylinders of fiberglass, aluminum, and stainless steel, all apparently open ended. They also tested a composite body resembling an actual payload. Eide tested closed-ended aluminum cylinders of 4:1, 8:1, 12:1, and 18:1 ℓ/r ratios.

In addition to these laboratory measurements, observations of the spin decay of satellites while in orbit have been compared with the theoretical decay rate assuming eddy current torque to be the responsible mechanism (References 9 and 10). Good correlation was obtained.

EQUIPMENT AND PROCEDURES

This investigation was carried on with the aid of the experimental apparatus shown in Figure 1. The specimen under test was installed at the center of the coil system and supported statically by a nonconducting column. The column in turn was supported by a highly sensitive torquemeter. Torques as low as 5 dyne-centimeters were measured, this limit being imposed by ambient noise (e.g., seismic vibrations and air currents). Test data were obtained by energizing the coil system with quadrature sinusoidal currents so as to produce a resultant magnetic vector, which rotated about a vertical axis. This induced eddy currents and consequent eddy-current torques in the stationary test specimen. The entire apparatus was encased in a plexiglass enclosure in order to minimize torque disturbance from air currents. The equipment itself was located in Quiet Lab No. 1 at the Goddard Space Flight Center Magnetic Test Facility, an isolated area where magnetic and seismic disturbances caused by automotive traffic and machinery are small. The specimens tested are listed in Table 2. No attempt was made to cancel the earth's ambient magnetic field during these tests since changes in the field would obviously have negligible effects on eddy-current torques.

A magnetometer survey was made in the coil system to check uniformity of field. Uniformity was found to be within 2 percent over the volume occupied by the largest test specimen.

Data were obtained at frequencies up to 1000 Hz with maximum flux levels of 0.94 gauss. Wave-form distortion in the coil currents became apparent at about 600 Hz and grew progressively worse with increased frequency. At these high frequencies, data were taken at lower flux levels to minimize distortion.

The torquemeter transducer (Reference 11) consisted of a set of parallel condenser plates arranged to form a differential capacitor. The application of torque to the meter caused a very slight rotation of its flexure pivots which resulted in an imbalance of the ac bridge of which the differential capacitor formed a part. The imbalance was proportional to the applied torque. Calibration was performed at frequent intervals, using an accurately known weight applied through a delicate bell crank mechanism so as to apply a known small force at a predetermined lever arm.

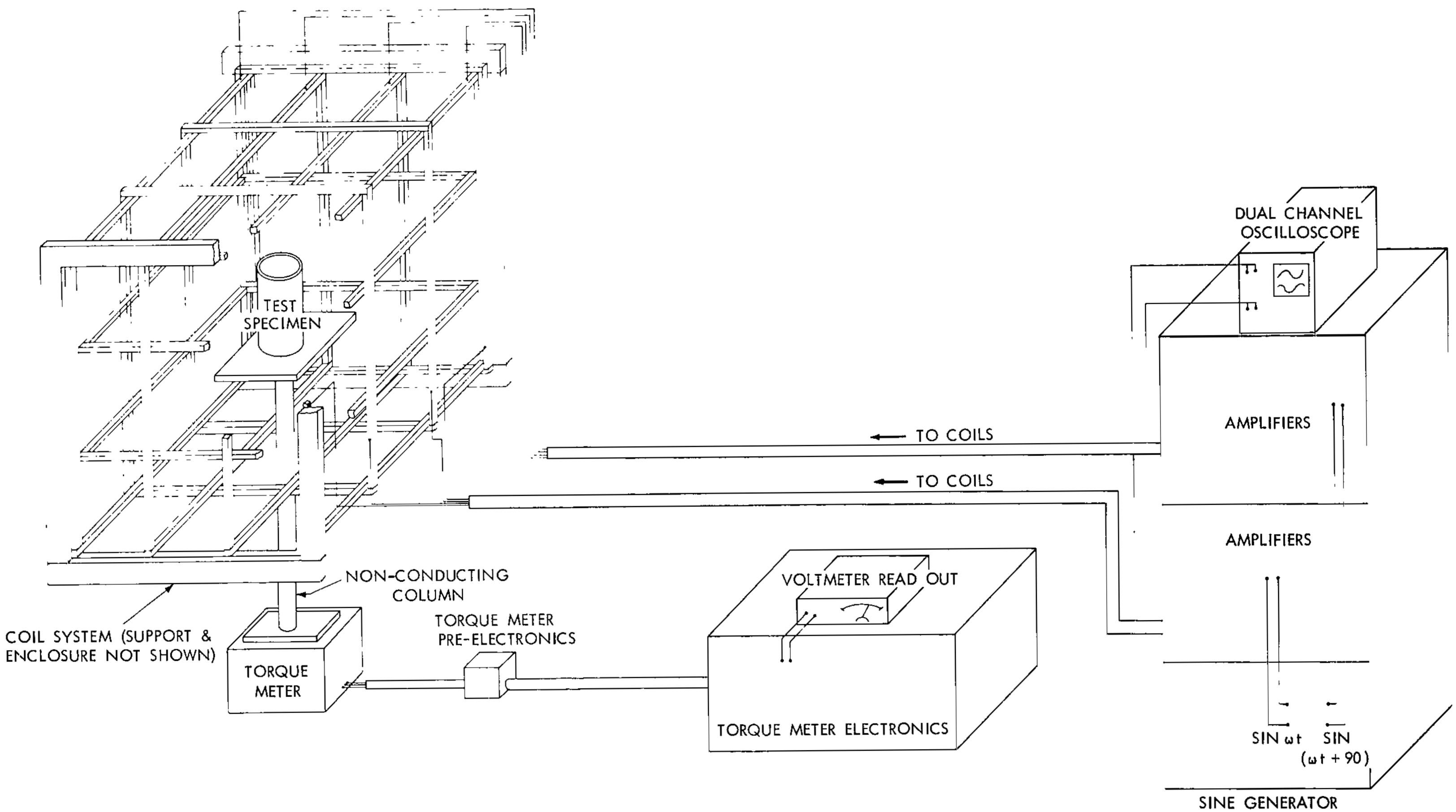

Figure 1—Schematic diagram of test apparatus.

Table 2

Specimen List.

Specimen Number	Specimen Shape	ℓ (inches)	r (inches)	Thickness (inches)	Material	Test Orientation (See Figure 2)	Test Data Figure Number
1	Sphere		3	0.05	Aluminum 6061		3
2	Open Cylinder	3	3	0.05	Aluminum 6061	2(a)	5
3	Open Cylinder	6	3	0.05	Aluminum 6061	2(a)	6, 27
4	Open Cylinder	9	3	0.05	Aluminum 6061	2(a)	7, 27
5	Open Cylinder	9	3	0.05	Aluminum 6061	2(a)	24, 25
6	Open Cylinder	9	3	0.05	Aluminum 6061	2(a) nested over specimen 12	23, 24, 25
7	Open Cylinder	3	3	0.05	Aluminum 6061	2(b)	8
8	Open Cylinder	6	3	0.05	Aluminum 6061	2(b)	9
9	Open Cylinder	9	3	0.05	Aluminum 6061	2(b)	10
10	Open Cylinder	6	3	0.05	304 Stainless	2(a)	11
11	Open Cylinder	6	3	0.05	304 Stainless	2(b)	11
12	Open Cylinder	6	2.85	0.05	Aluminum 6061	2(a)	23
13	Closed Cylinder	3	3	0.05	Aluminum 6061	2(a)	13
14	Closed Cylinder	6	3	0.05	Aluminum 6061	2(a)	14, 26
15	Closed Cylinder	9	3	0.05	Aluminum 6061	2(a)	15, 26
16	Closed Cylinder	3	3	0.05	Aluminum 6061	2(b)	16
17	Closed Cylinder	6	3	0.05	Aluminum 6061	2(b)	17
18	Closed Cylinder	9	3	0.05	Aluminum 6061	2(b)	18
19	Open Square	6	3*	0.05	Aluminum 6061	2(a)	19
20	Open Square	6	3*	0.05	Aluminum 6061	2(b)	20
21	Open Square	6	3*	0.25	Aluminum 6061	2(a)	21
22	Open Square	6	3*	0.25	Aluminum 6061	2(b)	22

*Half width.

Accuracy of data was affected by several factors:

1. Calibration

Calibrations were frequently performed during the taking of data. Repeatability was within 4 percent of the mean over the total testing period. Over short periods, such as from the beginning to the end of an individual test run, repeatability was within 2 percent of the mean. The mechanical calibrator was constructed to minimize pivot friction and to have accurately known lever arms. Calibration weights were checked on a laboratory balance. The error in applied torque was considered to be less than 1 percent of the mean.

2. Noise

Air currents and seismic vibration produced noise which limited the accuracy obtainable at low torque levels. By averaging three or more individual meter readings, a torque repeatability within ±5 dyne-centimeters was obtained.

3. Applied Field

The applied field was derived from knowledge of the coil constants and applied current which was determined by measuring the voltage drop across a precision resistor in the coil circuit. The inaccuracy in this method of measuring field strength is estimated at within 5 percent of the mean because of voltage reading error on the oscilloscope. As previously noted, homogeneity of field varied within 2 percent over the volume occupied by the largest test specimen.

4. Electrical Conductivity of Test Specimens

Test specimen conductivity varied from 45 percent of that of annealed copper, for the annealed 6061 aluminum alloy, to 40 percent for the T4 temper. The manufacturing process undoubtedly produced some strain hardening so the 40 percent figure was used. Error due to this source was estimated as zero to -5 percent. This is an error in the theoretical calculation as opposed to the experimental results.

5. Misorientation

The test specimens were oriented by eye either vertically or horizontally as shown in Figure 2. The cosine error incurred was estimated at ±1 percent-approximately 8 degrees.

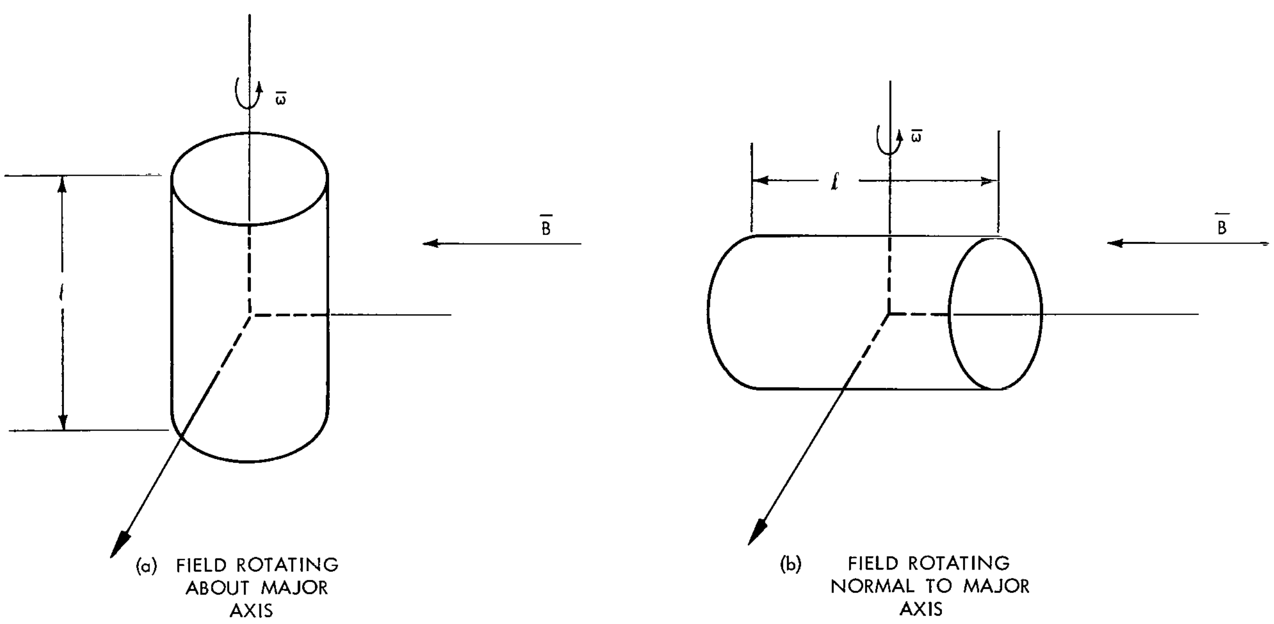

Figure 2—Orientation of test specimens in the magnetic field.

The probable overall error obtained by the square root of the sum of the squares of the individual errors is ±6 percent of the reading with a minimum error of ±5 dyne-centimeters. It is interesting to note that in the case of the sphere, theory and test agree to within 2 percent.

TEST RESULTS

Because the eddy-current torque varies as the square of the magnetic induction, plots were prepared of L/B^2* (dyne-centimeters per gauss squared) versus frequency in Hz for each of the individual specimens tested. These frequency response curves are Figures 3 through 22.

In addition, certain nested configurations were tested in which one cylinder was placed inside the other to gain some insight into shielding. The data obtained appear in Figures 23, 24, and 25.

Figures 26 and 27, in which torque is plotted against magnetic induction, show a quadratic relationship for various cylinders. This relationship was also verified for the other configurations.

Table 3 presents a comparison between theoretical and measured torque rates for low angular velocities (within the linear range).

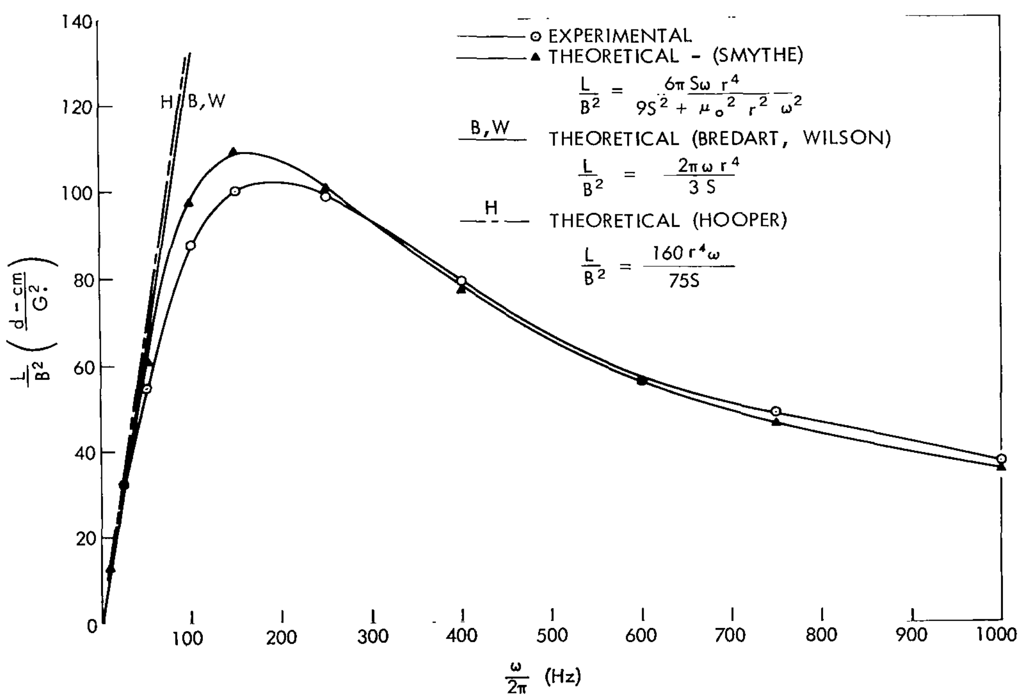

Figure 3—Theoretical versus experimental torque for a 6-inch diameter, 0.05-inch thick, aluminum sphere.

*Terms are defined in Appendix A.

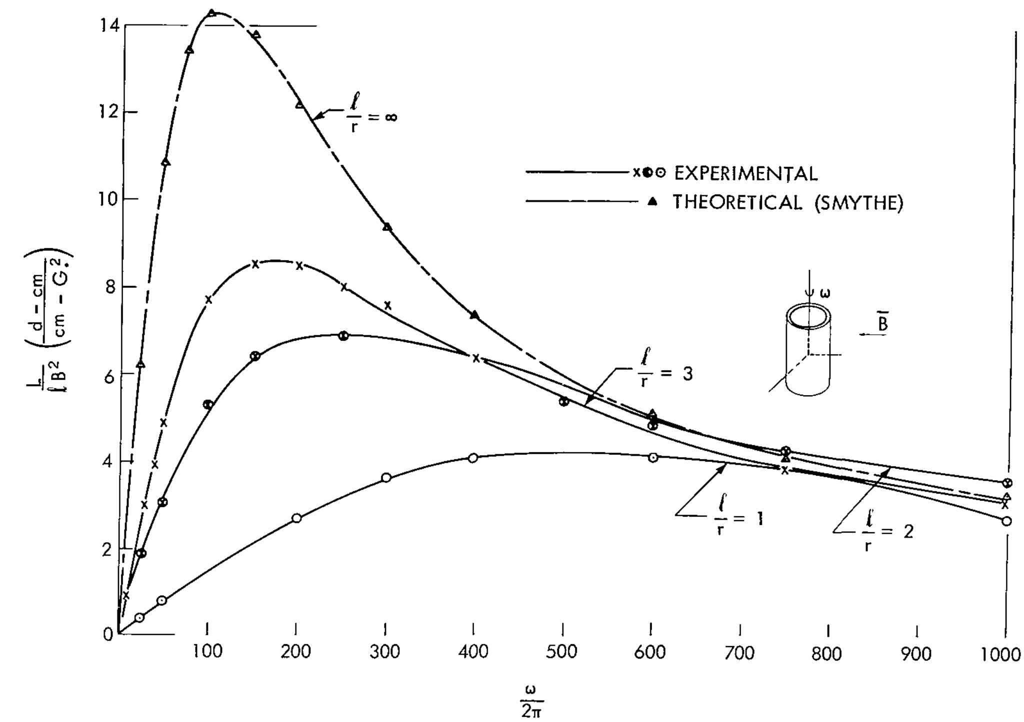

Figure 4—Torque comparison for open, 6-inch diameter, 0.05-inch thick, aluminum cylinders of various aspect ratios, ℓ/r.

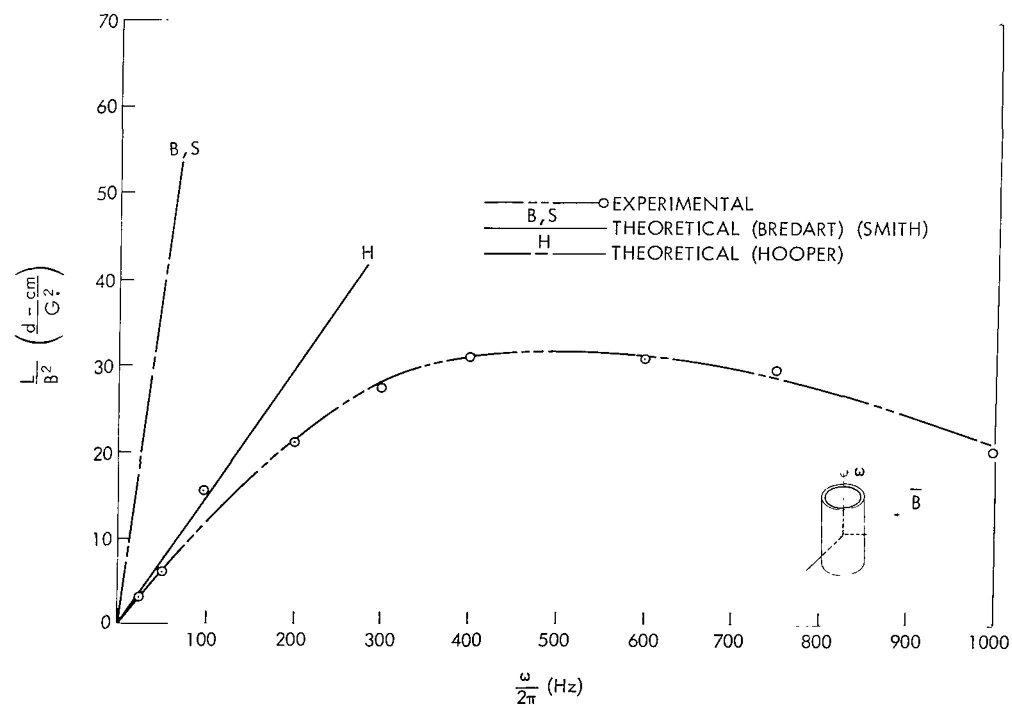

Figure 5—Theoretical versus experimental torque for an open, 6-inch diameter, 0.05-inch thick, 3-inch long, aluminum cylinder.

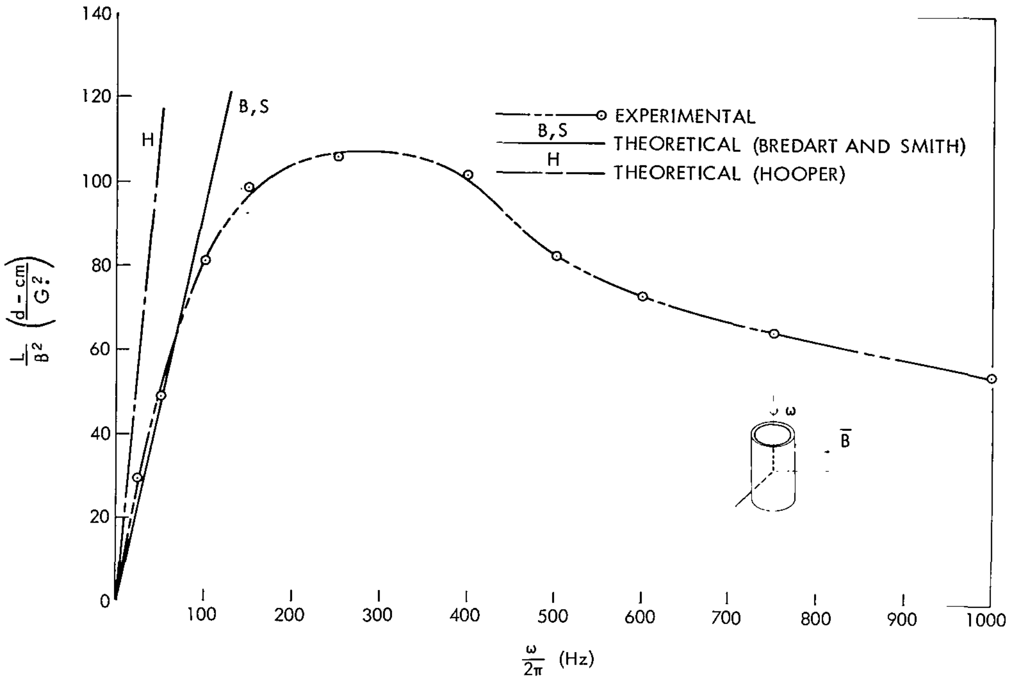

Figure 6—Theoretical versus experimental torque for an open, 6-inch diameter, 0.05-inch thick, 6-inch long aluminum cylinder.

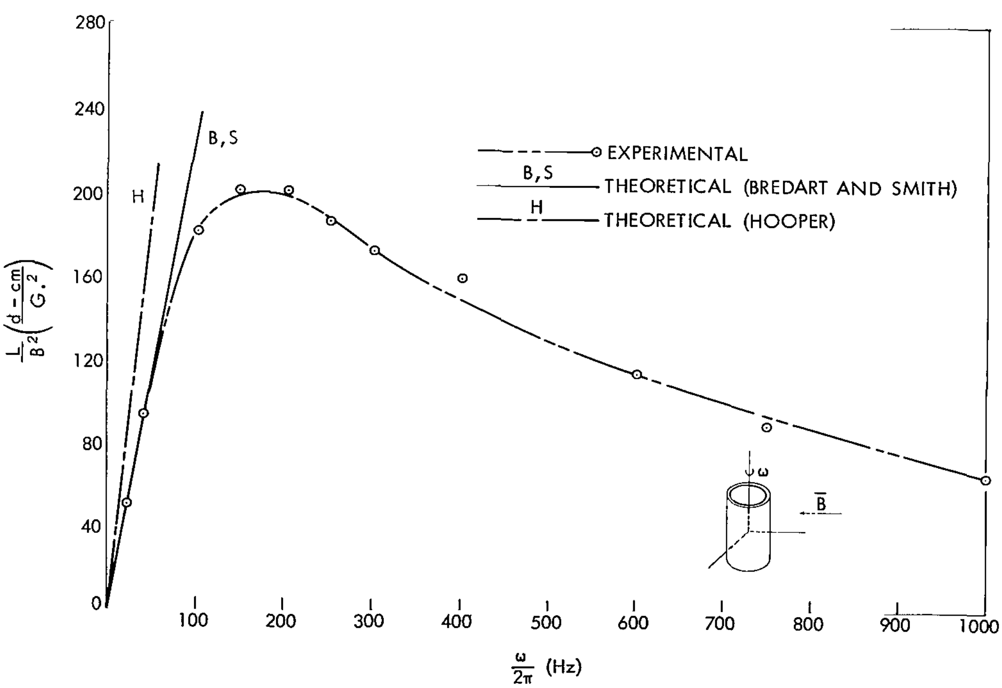

Figure 7—Theoretical versus experimental torque for an open, 6-inch diameter, 0.05-inch thick, 9-inch long, aluminum cylinder.

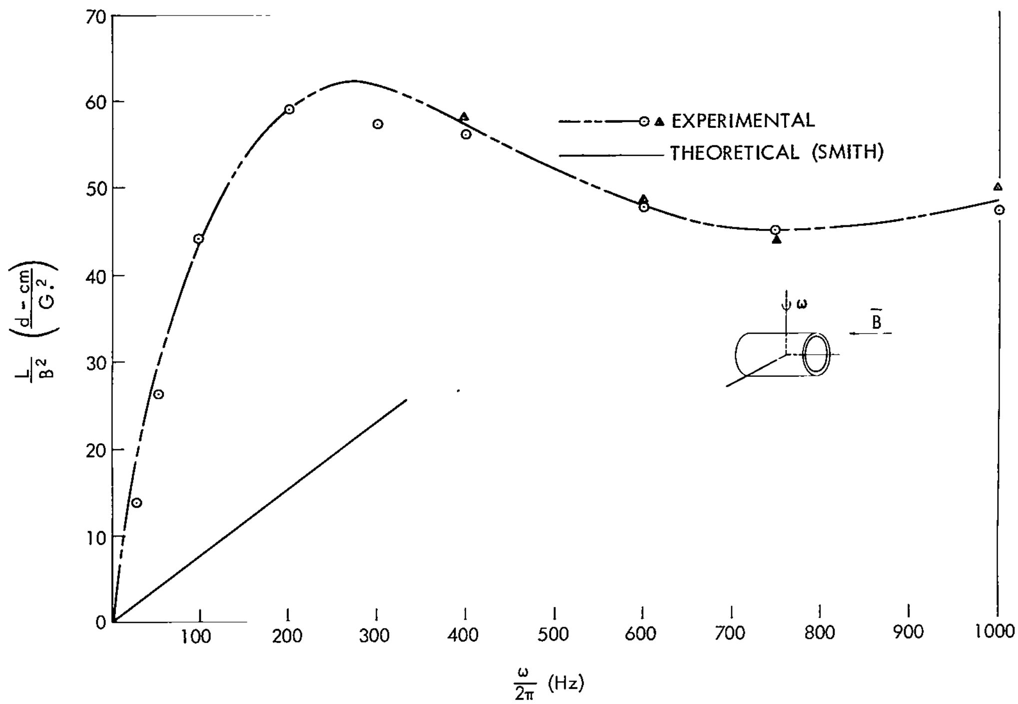

Figure 8—Theoretical versus experimental torque on an open 6-inch diameter, 0.05-inch thick, 3-inch long, aluminum cylinder.

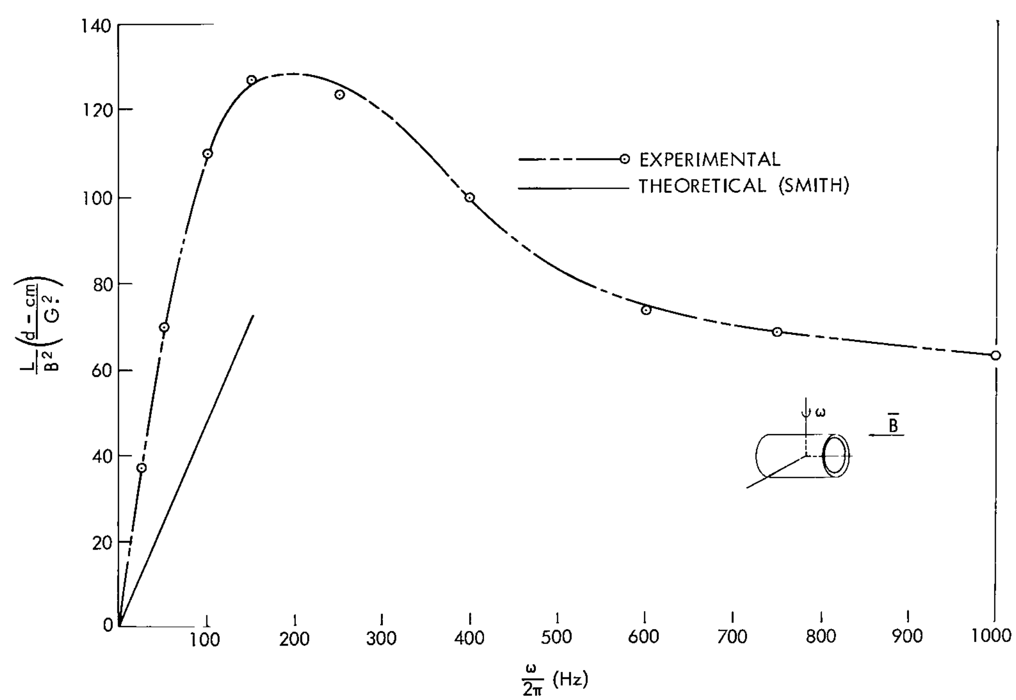

Figure 9—Theoretical versus experimental torque for an open, 6-inch diameter, 0.05-inch thick, 6-inch long, aluminum cylinder.

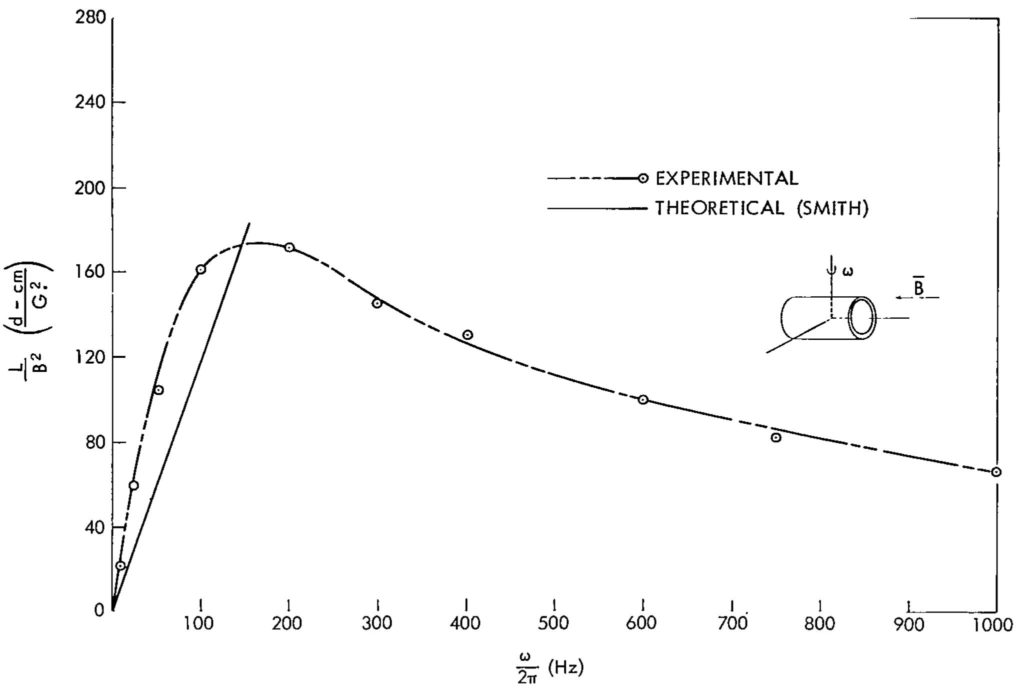

Figure 10—Theoretical versus experimental torque for an open, 6-inch diameter, 0.05-inch thick, 9-inch long, aluminum cylinder.

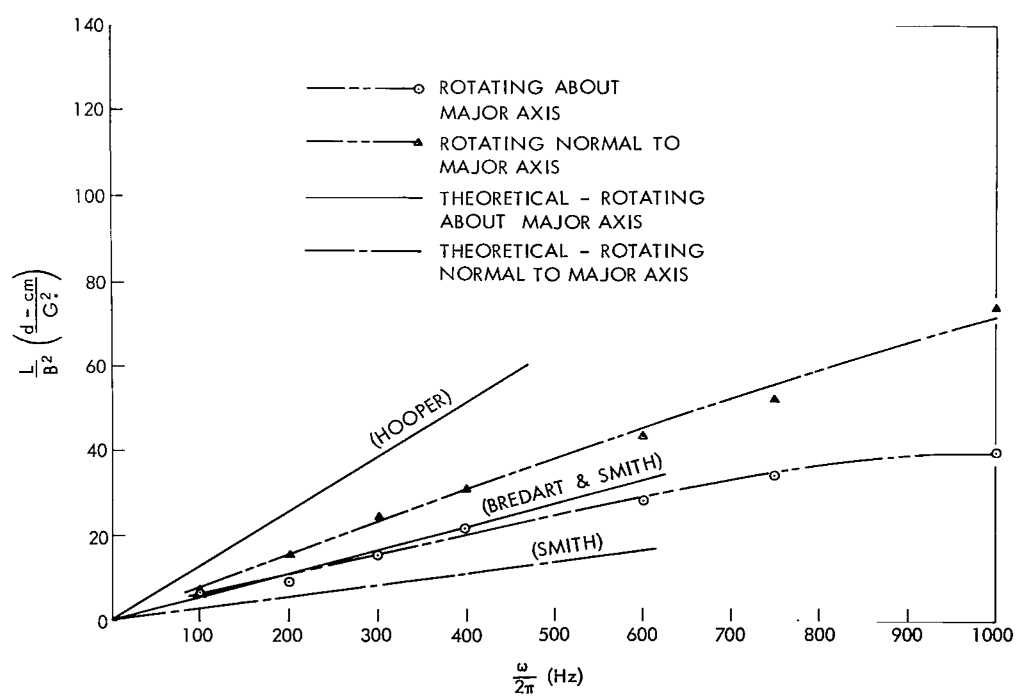

Figure 11—Theoretical versus experimental torque for an open, 6-inch diameter, 0.05-inch thick, 6-inch long, steel cylinder.

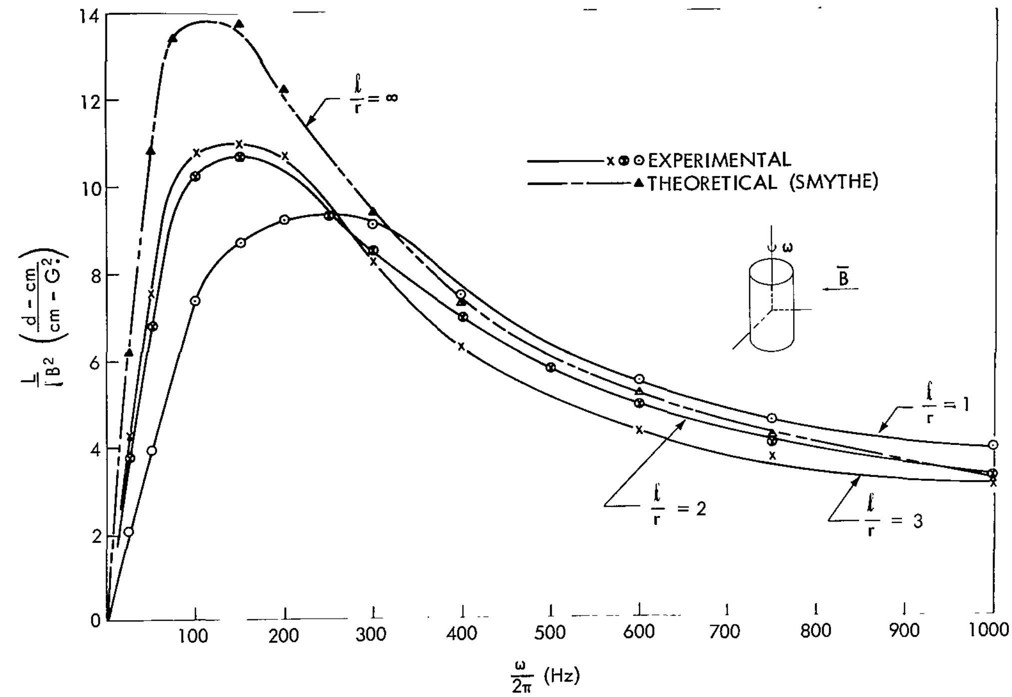

Figure 12—Torque comparison for closed, 6-inch diameter, 0.05-inch thick, aluminum cylinders for various aspect ratios, ℓ/r.

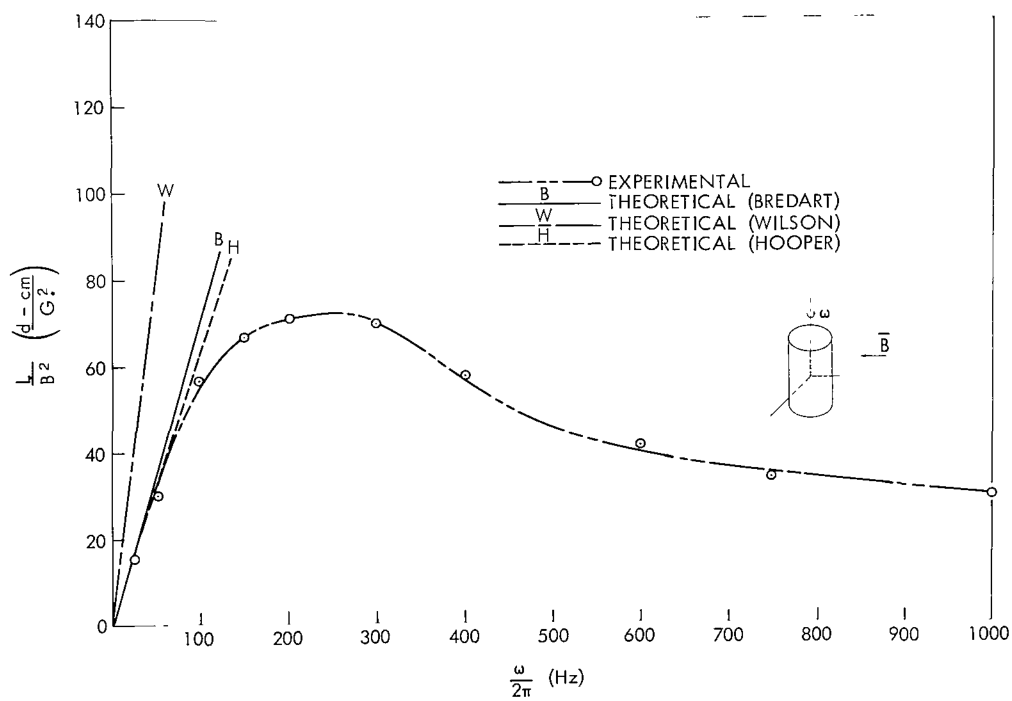

Figure 13—Theoretical versus experimental torque for a closed, 6-inch diameter, 0.05-inch thick, 3-inch long, aluminum cylinder.

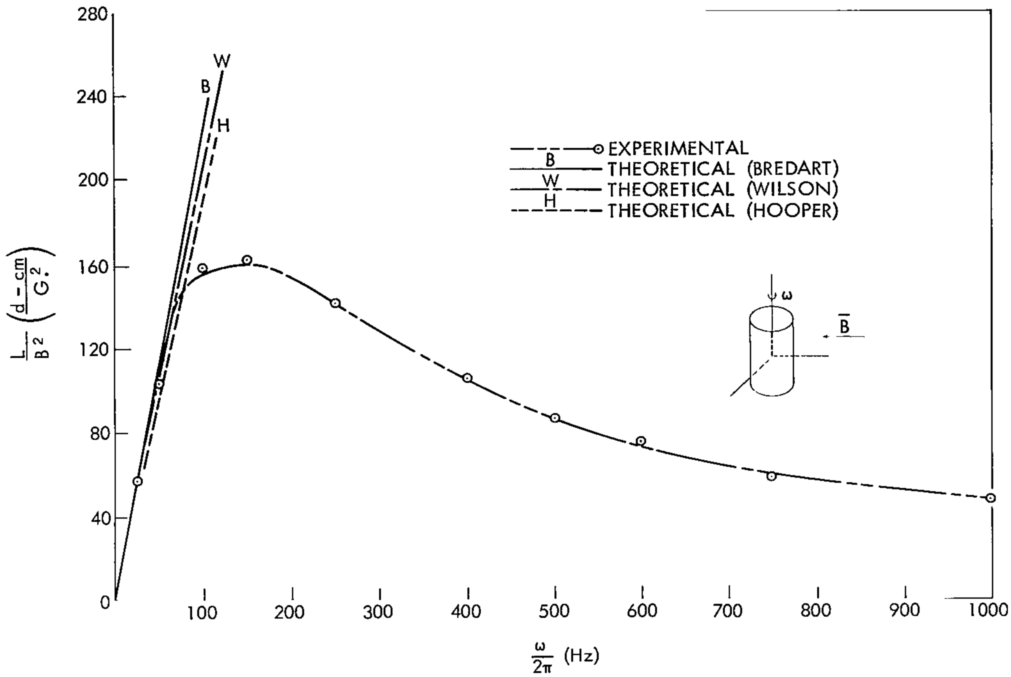

Figure 14—Theoretical versus experimental torque for a closed, 6-inch diameter, 0.05-inch thick, 6-inch long, aluminum cylinder.

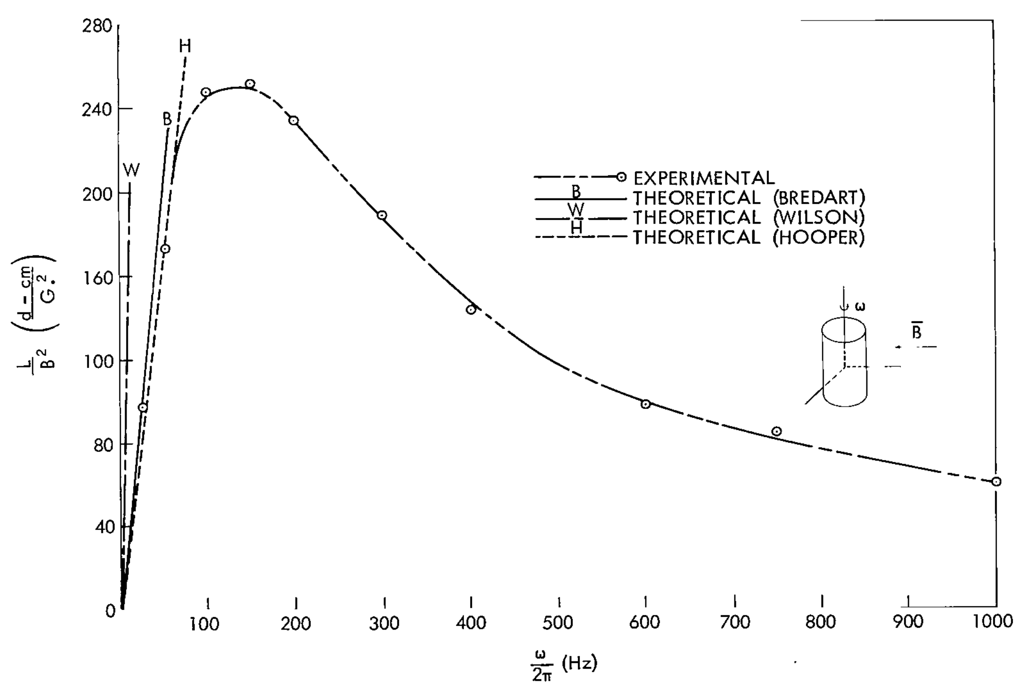

Figure 15—Theoretical versus experimental torque for a closed, 6-inch diameter, 0.05-inch thick, 9-inch long, aluminum cylinder.

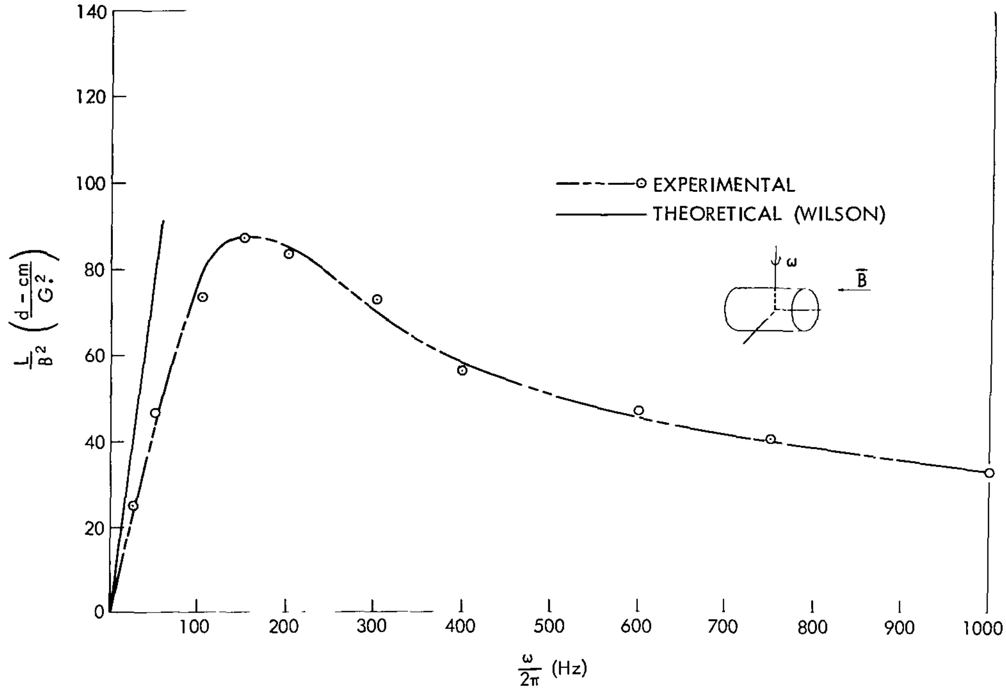

Figure 16—Theoretical versus experimental torque for a closed, 6-inch diameter, 0.05-inch thick, 3-inch long, aluminum cylinder.

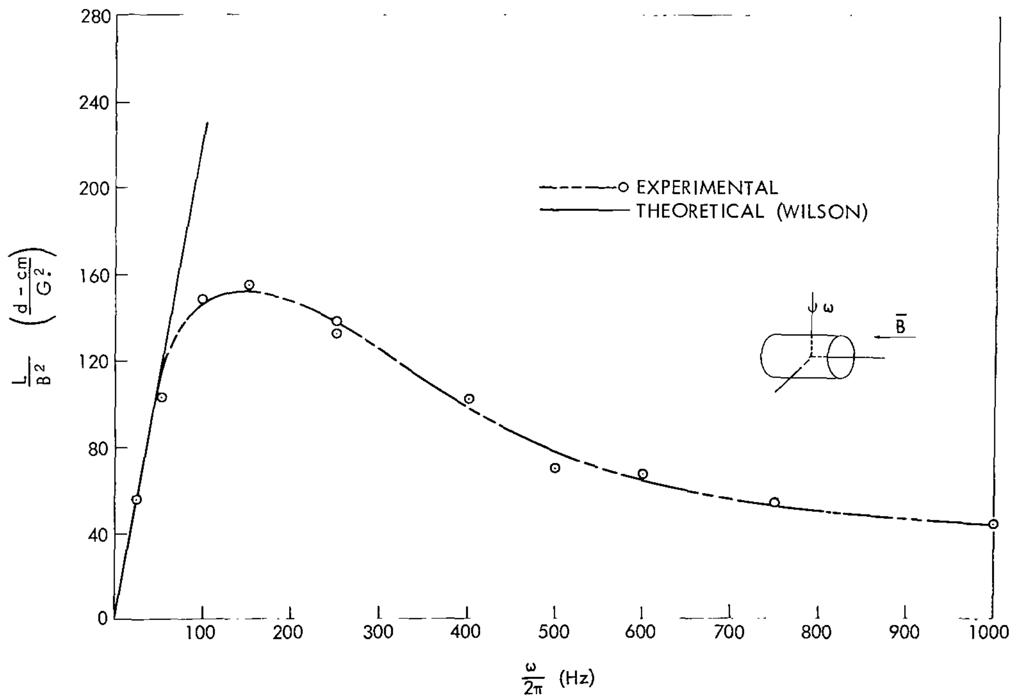

Figure 17—Theoretical versus experimental torque for a closed, 6-inch diameter, 0.05-inch thick, 6-inch long, aluminum cylinder.

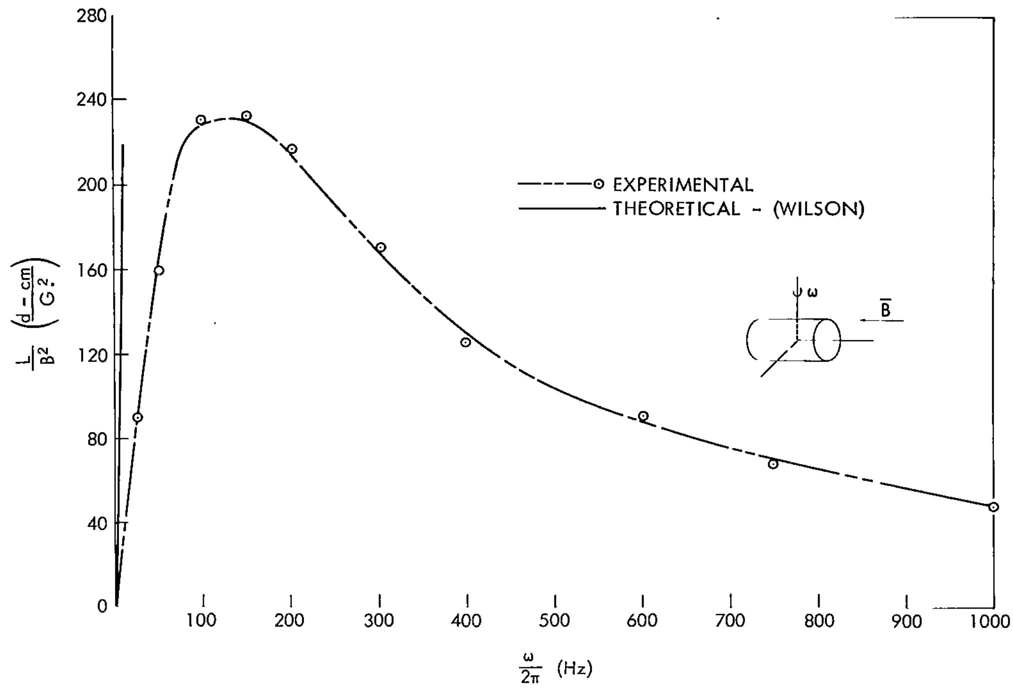

Figure 18—Theoretical versus experimental torque for a closed, 6-inch diameter, 0.05-inch thick, 9-inch long, aluminum cylinder.

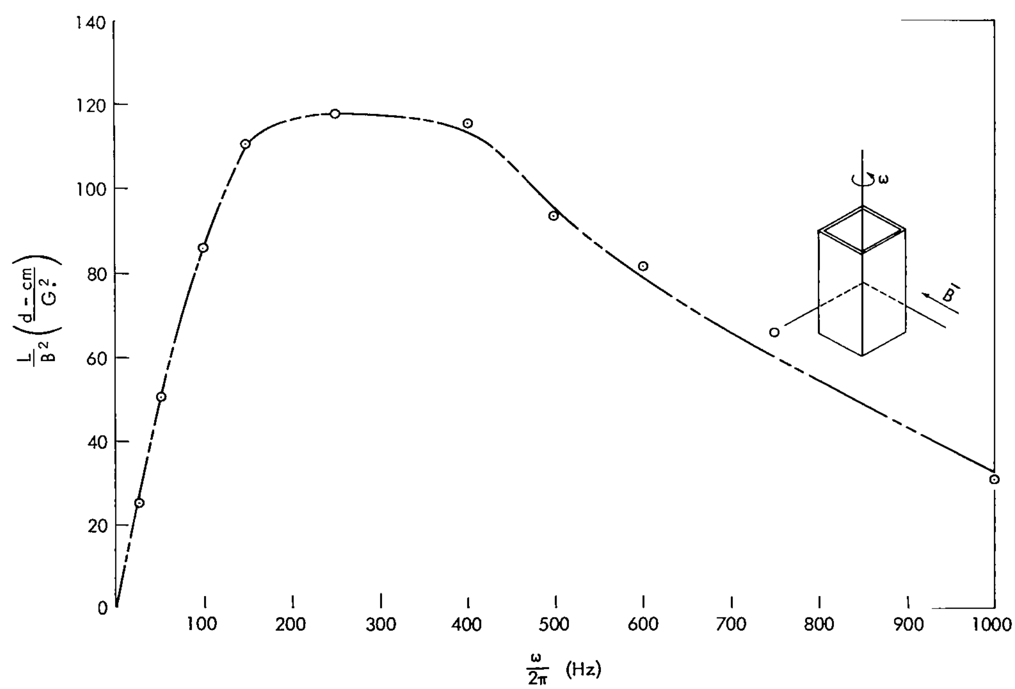

Figure 19—Experimental torque for an open, 6 inch by 6 inch, 0.05-inch thick, 6-inch long, square, aluminum tube, vertically oriented.

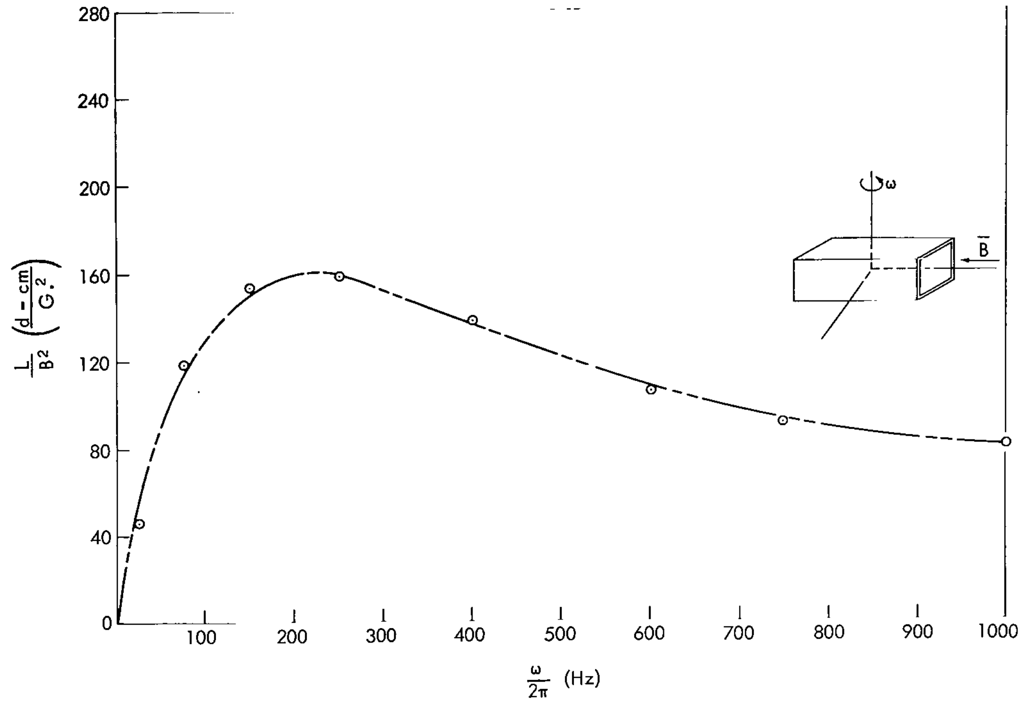

Figure 20—Experimental torque for an open, 6 inch by 6 inch, 0.05-inch thick, 6-inch long, square, aluminum tube, horizontally oriented.

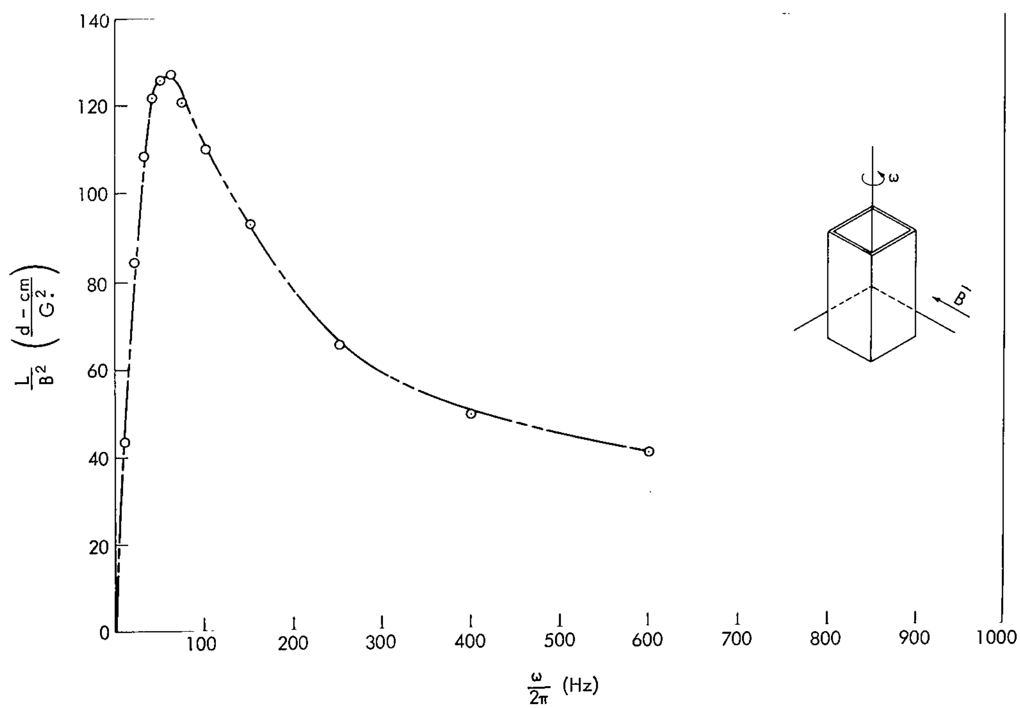

Figure 21—Experimental torque for an open, 6 inch by 6 inch, 0.25-inch thick, 6-inch long, square, aluminum tube, vertically oriented.

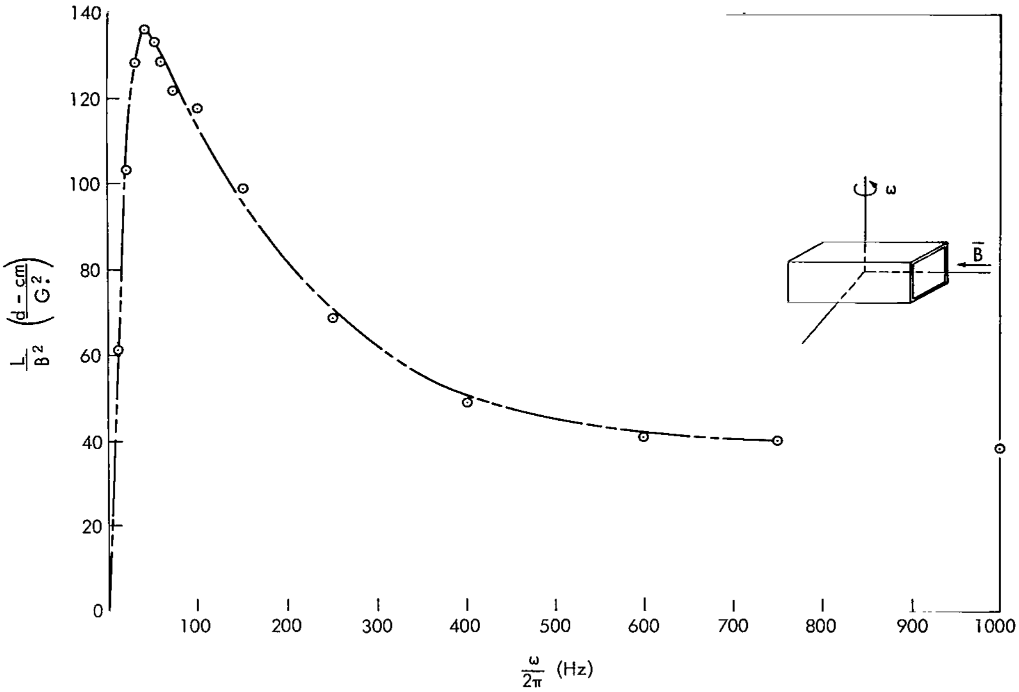

Figure 22—Experimental torque for an open, 6 inch by 6 inch, 0.25-inch thick, 6-inch long, square, aluminum tube, horizontally oriented.

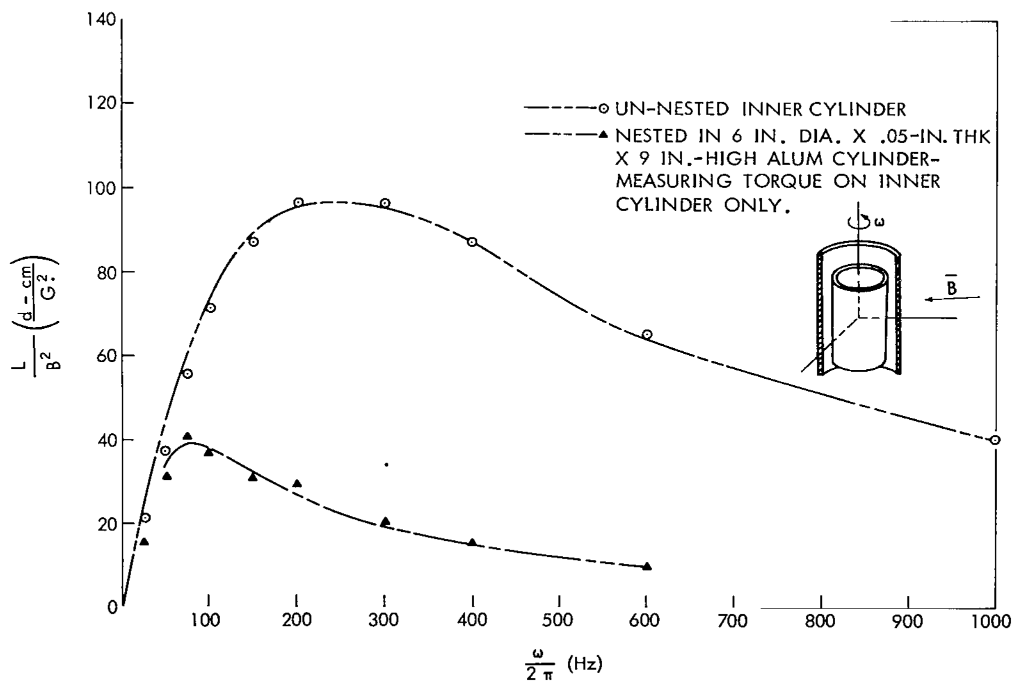

Figure 23—Experimental torque for an open, 5.7-inch diameter, 0.05-inch thick, 6-inch long, nested, aluminum cylinder.

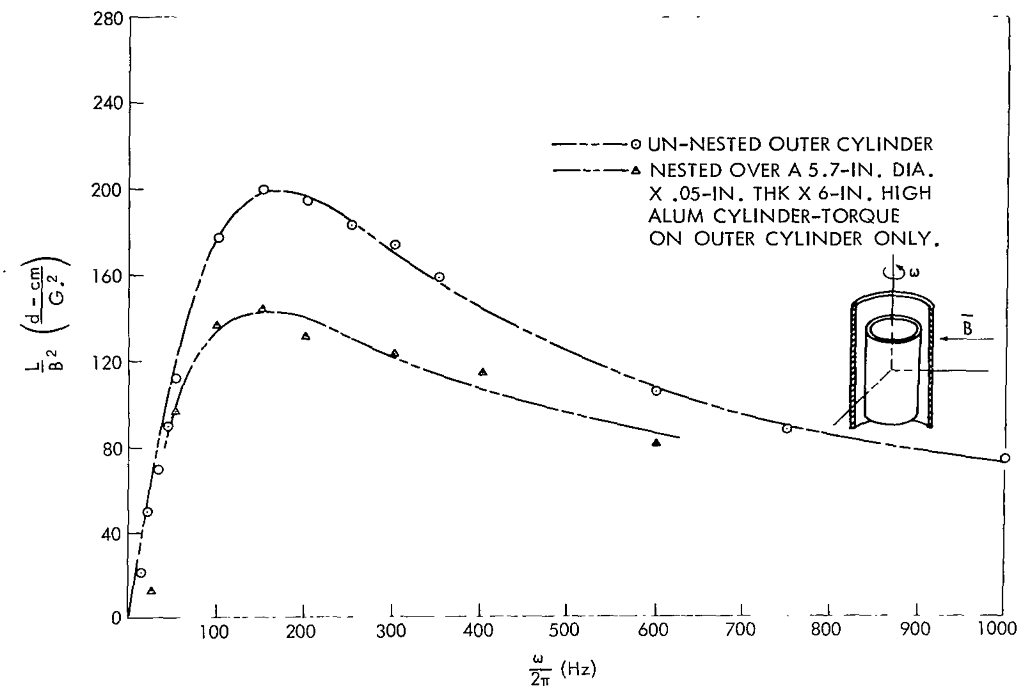

Figure 24—Experimental torque for an open, 6-inch diameter, 0.05-inch thick, 9-inch long, nested, aluminum cylinder.

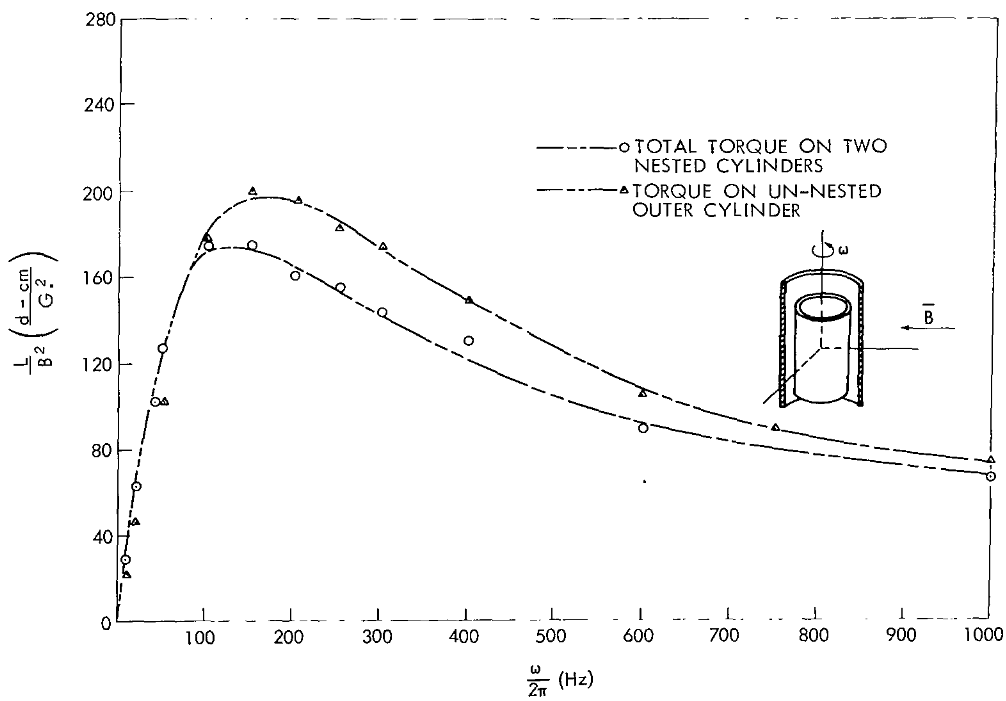

Figure 25—Experimental torque for an open, 5.7-inch diameter, 0.05-inch thick, 6-inch long, nested, aluminum cylinder in a 6-inch diameter, 9-inch long, aluminum cylinder.

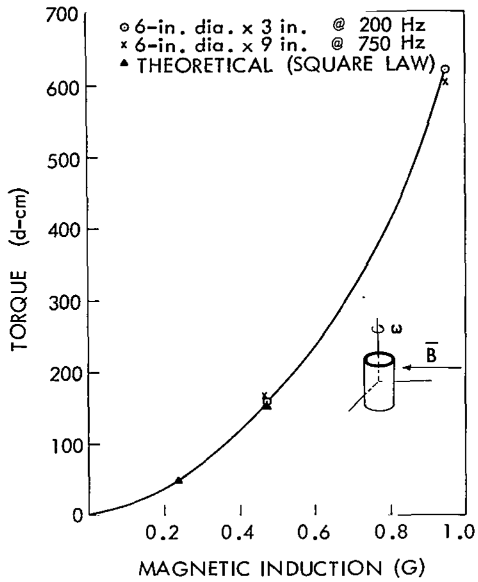

Figure 26—Theoretical versus experimental torque for closed aluminum cylinders.

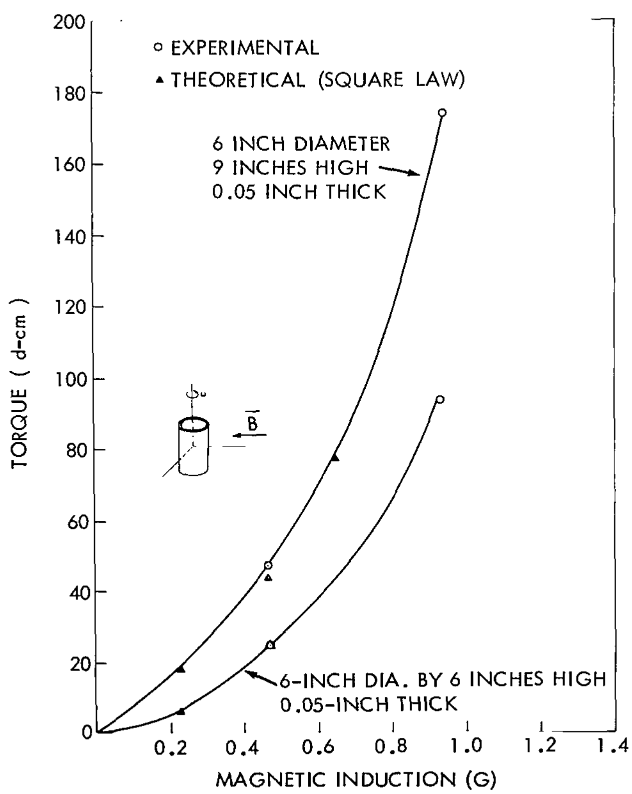

Figure 27—Theoretical versus experimental torque for two open aluminum cylinders.

Table 3

Ratio of Linear Damping Coefficients for Low Frequencies.*

Experimenter	Shape		Smythe (Reference 3)	Smith (Reference 6)	Bredart (Reference 8)	Hooper (Reference 5)	Wilson (Reference 7)
Eide (Reference 1)	Vertical Closed Cylinder	$\frac{\ell}{r} = 4$	$\frac{3.16}{1.77} = 1.78$	None	$\frac{2.39}{1.77} = 1.35$	$\frac{1.95}{1.77} = 1.10$	$\frac{33.7}{1.77} = 19$
		$\frac{\ell}{r} = 8$	$\frac{.395}{.298} = 1.32$	None	$\frac{.347}{.298} = 1.16$	$\frac{.270}{.298} = 0.91$	$\frac{22.3}{.298} = 75$
		$\frac{\ell}{r} = 12$	$\frac{.236}{.152} = 1.56$	None	$\frac{.216}{.152} = 1.42$	$\frac{.133}{.152} = 0.88$	$\frac{31.6}{.152} = 208$
		$\frac{\ell}{r} = 18$	$\frac{.035}{.024} = 1.45$	None	$\frac{.033}{.024} = 1.38$	$\frac{.023}{.024} = 0.96$	$\frac{10.5}{.024} = 438$
Juergensen (Reference 2)	Vertical Open Cylinder	Alum. $\frac{\ell}{r} = 11$	$\frac{132}{55.9} = 2.36$	$\frac{77}{55.9} = 1.38$	$\frac{77}{55.9} = 1.38$	$\frac{82.5}{55.9} = 1.47$	None
		Steel $\frac{\ell}{r} = 11$	$\frac{4.93}{4.01} = 1.23$	$\frac{4.01}{4.01} = 1.00$	$\frac{4.01}{4.01} = 1.00$	$\frac{4.29}{4.01} = 1.07$	None
Boyle, Mosher, and Greyerbiehl	Vertical Open Cylinder	$\frac{\ell}{r} = 1$	$\frac{2.01}{.124} = 16.3$	$\frac{.150}{.124} = 1.21$	$\frac{.150}{.124} = 1.21$	$\frac{.773}{.124} = 6.23$	None
		$\frac{\ell}{r} = 2$	$\frac{4.02}{.981} = 4.1$	$\frac{.948}{.981} = 0.97$	$\frac{.948}{.981} = 0.97$	$\frac{2.23}{.981} = 2.27$	None
		$\frac{\ell}{r} = 3$	$\frac{6.03}{2.32} = 2.6$	$\frac{2.37}{2.32} = 1.02$	$\frac{2.37}{2.32} = 1.02$	$\frac{3.92}{2.32} = 1.69$	None
	Vertical Closed Cylinder	$\frac{\ell}{r} = 1$	$\frac{2.01}{.602} = 3.34$	None	$\frac{.726}{.602} = 1.21$	$\frac{.660}{.602} = 1.10$	$\frac{1.63}{.602} = 2.71$
		$\frac{\ell}{r} = 2$	$\frac{4.02}{2.31} = 1.74$	None	$\frac{2.30}{2.31} = 0.99$	$\frac{1.98}{2.31} = 0.86$	$\frac{2.06}{2.31} = 0.89$
		$\frac{\ell}{r} = 3$	$\frac{6.03}{3.19} = 1.9$	None	$\frac{4.15}{3.19} = 1.30$	$\frac{3.55}{3.19} = 1.11$	$\frac{38.2}{3.19} = 12$
	Horizontal Open Cylinder	$\frac{\ell}{r} = 1$	None	$\frac{.075}{.556} = 0.13$	None	None	None
		$\frac{\ell}{r} = 2$	None	$\frac{.474}{1.48} = 0.32$	None	None	None
		$\frac{\ell}{r} = 3$	None	$\frac{1.19}{2.36} = 0.50$	None	None	None
	Horizontal Closed Cylinder	$\frac{\ell}{r} = 1$	None	None	None	None	$\frac{1.56}{1.00} = 1.56$
		$\frac{\ell}{r} = 2$	None	None	None	None	$\frac{2.28}{2.24} = 1.02$
		$\frac{\ell}{r} = 3$	None	None	None	None	$\frac{2.08}{3.59} = 0.58$
	Sphere		$\frac{1.32}{1.32} = 1.00$	None	$\frac{1.32}{1.32} = 1.00$	$\frac{1.34}{1.32} = 1.02$	$\frac{1.32}{1.32} = 1.00$

*Theoretical value/experimental value of dyne-cm/gauss^2 Hz.

DISCUSSION

For the thin-walled sphere, the theoretical expressions of Smythe, and Halversen and Cohen are applicable over the entire frequency range. The theoretical expressions of both Bredart and Hooper are limited to frequencies sufficiently low as to make distortion negligible. It can readily be seen that these latter expressions are in good agreement with the more general expressions as long as $9S^2 \gg \mu_v^2\, r^2\, \omega^2$. Table 3 and Figure 3 illustrate the excellent agreement obtained between theory and experiment over the entire frequency range tested.

For the other shapes tested, there is no high-frequency theory available except that of Smythe for the torque per unit length on an infinitely long cylinder. It can be noted, however, that in every case the general behavior of the torque as a function of frequency is the same: the torque rises to a maximum value, then tails off at higher frequencies.

An examination of Table 3 reveals that the formulas of Bredart for open- and closed-end cylinders spinning about their major axes are more consistently in agreement with experiment than those of Hooper and Wilson. For a cylinder spinning about an axis normal to its major axis, agreement is poor except for Wilson's formula for the closed-end cylinder of $\ell/r = 2$. Regarding the open-ended cylinder spinning about an axis normal to its major axis there appears to be a trend indicating better agreement between Smith's theoretical formula and experiment at higher ℓ/r ratios.

As stated above, no high-frequency theory exists except for the infinitely long cylinder spinning about its major axis. However, if we assume the general form of the equation to remain unchanged, we may modify Smythe's formula to obtain

$$\frac{L}{B^2} = \frac{A\,\omega\, s\, r^3 \ell}{CS^2 + \mu_v^2\, r^2\, \omega^2},$$

where A and C are constants which are functions of the fineness ratio, having the values 4π and 4 respectively for the infinite cylinder. Figures 28 and 29 present plots of these constants, which as may be seen, appear to be trending to the infinite cylinder values as the ℓ/r ratio is increased.

Although no theory is available for the torque on the specimens of square cross section tested, it is evident from Figures 19 through 22 that the shape of the frequency response curve is similar to that of the circular cylinders.

The results of experiments with nested cylinders are shown in Figures 23, 24, and 25. The effect of shielding on the inner cylinder is evident from the two curves of Figure 23. Figure 23 shows that the torque on the outer or shielding cylinder is also reduced when the two are nested. Rather surprisingly, Figure 25 indicates that above the linear range, the total torque on the pair of nested cylinders was less than the torque on the unnested outer cylinder. The shielding effect

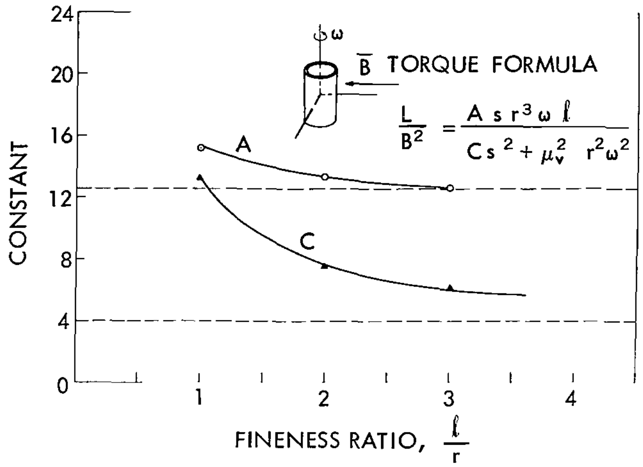

Figure 28—Empirical constants A and C as a function of fineness ratio for a closed, 6-inch diameter, 6-inch long, 0.05-inch thick, aluminum cylinder.

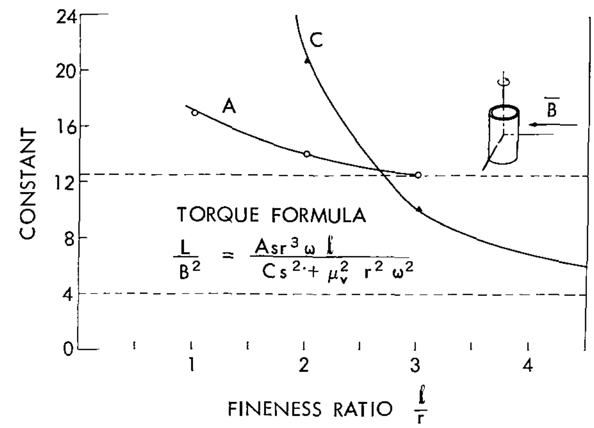

Figure 29—Empirical constants A and C as a function of fineness ratio for an open 6-inch diameter, 6-inch long, 0.05-inch thick, aluminum cylinder.

is a function of frequency, being negligible in the low frequency range and a maximum in the vicinity of the peak response of the unnested members.

CONCLUSIONS

The present investigation has verified theoretical predictions that eddy-current torques will peak and then tail off as the rotational frequency is increased. However, the spin rates of present day spacecraft are sufficiently low that the linear approximations commonly used in the low frequency range are good enough. For example, a 48-inch diameter spherical satellite made of 0.05 inch aluminum alloy would have its peak eddy-current torque at about 1200 rpm whereas the great majority of satellites have spin rates less than 200 rpm. Under these circumstances the principal utility of this investigation is to present the designer with an opportunity to compare the several theoretical torque expressions available with the experimental data in the linear range. As can be seen from Table 3, a rather wide divergence exists.

The investigation into shielding effects shows that, at the normal spin frequencies of spacecraft, the distortion of the ambient field due to eddy currents is negligible. Thus it is quite proper to calculate the eddy-current torque contributions from each component of the spacecraft without regard to interactions, and to sum them to get the total retarding torque.

A further consideration is the production of eddy-current torques in spinning elements on board the spacecraft. For example, momentum wheels, unless located within a housing of high magnetic permeability, will have eddy-current torques induced within them by interaction with the ambient magnetic field. Such devices usually rotate at high angular velocities, and, if torques are calculated on the basis of linear dependence on angular velocity, they may be grossly in error.

It would appear that eddy-current torques may be much more significant for Jupiter probes than terrestrial satellites if present estimates of the Jovian magnetic field are correct. In that

event, investigations which test theory by experiment or which provide empirical data in the absence of theory will contribute to the soundness of design of such attitude control systems.

Goddard Space Flight Center
National Aeronautics and Space Administration
Greenbelt, Maryland, October 4, 1968
125-19-03-05-51

REFERENCES

1. Eide, D. G., "Experimental Evaluation of the Deceleration of Aluminum Cylinders Rotating in a Magnetic Field and Comments on Magnetic Damping of a Flywheel Control," NASA Technical Note D-749, April 1961.

2. Juergensen, K., et al., "Experiments in Damping a Rotating Satellite in Magnetic Fields," Army Ballistic Missile Agency Report DG-M-3-58, April 1958.

3. Smythe, W. R., "Static and Dynamic Electricity," 2nd Edition, McGraw-Hill Book Company, 1950.

4. Halverson, R. P., and Cohen, H., "Torque on a Spinning Hollow Sphere in a Uniform Magnetic Field," IEEE Trans. Aerospace Navigational Electron., 11(2):118-127, June 1964.

5. Hooper, J. W., "The Damping of Metallic Cylindrical and Spherical Bodies Rotating in a Uniform Magnetic Field," Army Ballistic Missile Agency, Technical Report DG-R-15, November 1957.

6. Smith, G. L., "A Theoretical Study of the Torques Induced by a Magnetic Field on Rotating Cylinders and Spinning Thin-Wall Cones, Cone Frustums, and General Body of Revolution," NASA Technical Report R-129, 1962.

7. Wilson, R. H. Jr., "Rotational Magnetodynamics and Steering of Space Vehicles," NASA Technical Note D-566, September 1961.

8. Bredart, G., "Etude du Couple Retardateur Produit par L'Interaction du Champ Magnetique Terrestre et des Courants de Foucalt Induits Dans un Satellite en Rotation," Revue MBLE, Vol. 8, pp. 3-19, March 1965.

9. Wilson, R. H. Jr., "Rotational Decay of the Satellite 1960 ETA 2 Due to the Earth's Magnetic Field," NASA Technical Note D-1469, October, 1962.

10. Bandeen, W. R., and Manger, W. P., "Angular Motion of the Spin Axis of the Tiros I Meteorological Satellite Due to Magnetic and Gravitational Torques," NASA Technical Note D-571, April 1961.

11. "Manufacture of a Sensitive Angle Measuring System," Fairchild Hiller Corp. Report PCD-TR-67-1, (prepared under NASA contract NAS 5-9383) Farmingdale, N. Y., February 1967.

12. Goldstein, K. S., and Gray, G. R., "Handbook of Definitions, Terms, Formulas, Conversion Tables, and Measurement Methods for Magnetic Phenomena," Texas Instrument Co., Report 2-61042-2 (prepared for Jet Propulsion Laboratories under contract No. BE4-217626), Dallas, Texas, December 1963.

Appendix A

Units and Constants

Table A1 is a listing of symbols, conversions, and constants used both in this report and in the reference reports with their units listed in both the MKS and CGS systems. An excellent review of the development of the various systems of units, with conversion tables, can be found in Reference 12.

Table A1

Symbols, Conversions, and Constants.

Quantity	Symbol	Units*		Value (when constant)		Comments
		RMKS	CGS	RMKS	CGS	
Length	h, ℓ	meter	centimeter	—	—	—
Half-length	h	meter	centimeter	—	—	—
Radius	a, r, R	meter	centimeter	—	—	—
Inner radius	r_i	meter	centimeter	—	—	—
Outer radius	r_o	meter	centimeter	—	—	—
Thickness	e, Δr, T	meter	centimeter	—	—	—
Angular velocity	ω	$\frac{\text{radians}}{\text{second}}$	$\frac{\text{radians}}{\text{second}}$	—	—	—
Electrical conductivity	σ	mhos/ meter	abmhos/cm*	alum (6061) = 2.39×10^7 s.s. 304 = 1.39×10^6	2.39×10^{-4} 1.39×10^{-5}	—
Surface resistivity	S	ohms	abohms*	—	—	$S = \frac{1}{\sigma \Delta r}$
Permeability	μ_v	henry/ meter	unitless	$4\pi \times 10^{-7}$ for vacuum	1 for vacuum	—
Magnetic field intensity	h, H	$\frac{\text{amp-turns}}{\text{meter}}$	oersted	—	—	—
Magnetic flux density (induction)	B	$\frac{\text{weber}}{\text{meter}^2}$	gauss	—	—	$1G. = 10^{-4} \frac{w}{m^2}$
Torque per unit field squared	$\frac{L}{B^2}$	$\frac{\text{newton-meter}}{(\text{weber/meter}^2)^2}$	$\frac{\text{dyne-centimeter}}{\text{gauss}^2}$	—	—	$10 \frac{\text{n-m}}{[\text{w/m}^2]^2} =$ 1 d-cm/G.^{2}
Speed of light	C	$\frac{\text{meters}}{\text{second}}$	$\frac{\text{centimeters}}{\text{second}}$	3×10^8	3×10^{10}	Used in Gaussian System

*Smith (Reference 6) works in the Gaussian System in which resistivity is measured in statohms. The conversion is: $\text{ohms} \times \frac{1.113}{10^{12}} = \text{statohms}$

Appendix B

Reference Formulas Taken from Sources

The formulas as written by the referenced authors were all converted to a common terminology in the RMKS system in Table 1. In addition to converting all equations to the RMKS system, certain substitutions were made. To assist in understanding the transition, the equation as originally written and the substitutions made are presented in Table B1.

Substitutions made:

$$\text{since } \left(r_0 - r_i\right) \ll r_0$$

$$r_0 \times r_i \cong r_0^2 \cong r^2$$

$$r_0 - r_i = \text{thickness}$$

$$\sigma \times \text{thickness} = \frac{1}{S}$$

$$\mu H = B$$

Table B1

Eddy-Current Torque Formulas for Thin Shell Bodies of Revolution with the Magnetic Field Applied at 90° to the Spin Axis.

Configuration	Smythe (Reference 3)	Smith (Reference 6)	Bredart (Reference 8)	Hooper (Reference 5)	Wilson (Reference 7)
Sphere	$\frac{6\pi B^2 S \omega a^4}{9S^2 + \mu_v^2 a^2 \omega^2}$ [Also by Halverson and Cohen, Reference 4]	None	$\frac{2}{3}\pi \sigma \omega R^4 B^2 e$	$\frac{32}{75} \frac{\mu^2 H_0^2 \omega \sigma}{(r_0^5 - r_i^5)^{-1}}$	$\frac{2}{3} \sigma \pi \mu^2 H^2 \omega r^4 \Delta r$
Vertical Open Cylinder	$\frac{4\pi \omega S a^3 B^2}{4S^2 + \omega^2 \mu_v^2 a^2}$ *	$\frac{\pi \sigma h^2 \omega r^3 \ell \tau}{C^2 \left(1 - \frac{2r}{\ell} \mathrm{TANH} \frac{\ell}{2r}\right)^{-1}}$ †	$\frac{2\pi \sigma \omega R^3 B^2 e h}{\left(1 - \frac{R}{h} \mathrm{TANH} \frac{h}{R}\right)^{-1}}$ ‡	$\frac{\pi(\mu^2 H_0^2 \ell^2 \omega \sigma) 10^{-9}}{4\left[\ell + \frac{\pi}{4}(r_0 + r_i)\right](r_0^4 - r_i^4)^{-1}}$ §	None
Vertical Closed Cylinder	$\frac{4\pi \omega S a^3 B^2}{4S^2 + \omega^2 \mu_v^2 a^2}$ *	None	$\frac{2\pi \sigma \omega R^3 B^2 e h}{\left(1 - \frac{\frac{R}{h} \mathrm{TANH} \frac{h}{R}}{1 + \mathrm{TANH} \frac{h}{R}}\right)^{-1}}$ ‡	$\frac{\pi(\mu^2 H_0^2 \ell^2 \omega \sigma) 10^{-9}}{4\left[\ell + (r_0 + r_i)\right](r_0^4 - r_i^4)^{-1}}$ §	$K < 1$ ‖ $\sigma \mu^2 H^2 \omega h^4 K \left[\frac{\pi}{4}\left(\frac{3}{K} + 1 + \frac{K}{2}\right) - \left(1 + \frac{1}{2 - 2K}\right) - \frac{3 - 4K}{K(1-K)\sqrt{1-K^2}} \mathrm{TAN}^{-1} \frac{\sqrt{1-K^2}}{1+K}\right] \Delta r$ $K > 1$ $\sigma \mu^2 H^2 \omega h^4 K \left[\frac{\pi}{4}\left(\frac{3}{K} + 1 + \frac{K}{2}\right) - \left(1 + \frac{1}{2 - 2K}\right) - \frac{3 - 4K}{2K(1-K)\sqrt{K^2-1}} \mathrm{LOG}_e \left(K + \sqrt{K^2 - 1}\right)\right] \Delta r$ $K = 1$ $\left(18\pi - \frac{160}{3}\right) \sigma \mu^2 H^2 \omega r^4 \Delta r$
Horizontal Closed Cylinder	None	None	None	None	$\frac{1}{2}$ Corresponding Value of Vertical Cylinder Plus $\frac{1}{4} \sigma \pi \mu^2 H^2 \omega \left(\frac{1}{2} r + h\right) r^3 \Delta r$
Horizontal Open Cylinder	None	$\frac{\pi \sigma h^2 \omega r^3 \ell \tau}{2C^2 \left(1 - \frac{2r}{\ell} \mathrm{TANH} \frac{\ell}{2r}\right)^{-1}}$ †	None	None	None

*Torque per unit length for an infinite length.

†Gaussian units h is field intensity (Gauss).

‡$h = \ell/2$.

§Measurements are in CGS units.

‖$K = 2r/h$.